

Dynamic Avatar-Scene Rendering from Human-centric Context

Wenqing Wang, Haosen Yang, Josef Kittler, Xiatian Zhu

Abstract—Reconstructing dynamic humans interacting with real-world environments from monocular videos is an important and challenging task. Despite considerable progress in 4D neural rendering, existing approaches either model dynamic scenes holistically or model scenes and backgrounds separately aim to introduce parametric human priors. However, these approaches either neglect distinct motion characteristics of various components in scene especially human, leading to incomplete reconstructions, or ignore the information exchange between the separately modeled components, resulting in spatial inconsistencies and visual artifacts at human-scene boundaries. To address this, we propose Separate-then-Map (StM) strategy that introduces a dedicated information mapping mechanism to bridge separately defined and optimized models. Our method employs a shared transformation function for each Gaussian attribute to unify separately modeled components, enhancing computational efficiency by avoiding exhaustive pairwise interactions while ensuring spatial and visual coherence between humans and their surroundings. Extensive experiments on monocular video datasets demonstrate that StM significantly outperforms existing state-of-the-art methods in both visual quality and rendering accuracy, particularly at challenging human-scene interaction boundaries. We provide demo videos in supplementary and the code will be released upon acceptance.

Index Terms—4D reconstruction and animation, digital human avatar, 4D gaussian splatting.

I. INTRODUCTION

HUMAN-CENTRIC monocular videos, which capture people interacting with real-world environments, are a common data source for applications such as AR/VR, visual effects, gaming, and simulation. While much progress has been made in reconstructing isolated human avatars in clean backgrounds [3, 4, 5, 6, 7, 8, 9], relatively less attention has been given to rendering humans together with their surrounding environments, which is essential for modeling realistic human-scene interactions.

Recent works [1, 2, 10, 11, 12, 13, 14] attempt to reconstruct human-centric scenes by jointly modeling the human and background. These approaches can be broadly classified into two distinct methodologies. One line of work, represented by holistic 4D scene modeling approaches [1, 10, 12, 15, 16], employs a unified 4D representation to model the entire scene, thereby requiring the simultaneous capture of drastically different motion patterns, specifically, fast-moving humans with complex articulated poses and static or slowly-changing backgrounds. This inherent conflict in motion characteristics impedes effective disentanglement and reconstruction of foreground and background components, particularly under the

large motions, complex poses, and limited viewpoints typical of monocular videos [8]. As evident in Figure 1(a), this holistic strategy leads to instability for dynamic object reconstruction.

Alternatively, a more effective approach explicitly separates the human and background into independently modeled components, as demonstrated in [2, 11, 13, 14]. This decomposition benefits from human-specific priors (e.g., SMPL [17], FLAME [18]), which provide strong constraints for accurately modeling human motion and articulation, but also introduces new challenges when the separately reconstructed components are combined. For example, recent work [2] combining 3D Gaussian Splatting (3DGS) with parametric-based human-deformable Gaussian Splatting to represent the scene and human avatar separately, ultimately merging the two independent models through direct concatenation. This type of direct merging strategy introduces floating artifacts and partial occlusions at the interaction boundaries (Figure 1(b)). These issues arise due to separate initialization and differing design and optimization strategies, which hinder information integration between the two components.

To overcome this largely overlooked issue, we propose **Separate-then-Map** (StM) strategy for human-centric 4D scene reconstruction, as shown in Figure 1(c). Unlike previous separate-based methods that directly concatenate independently optimized components, our approach introduces a dedicated information mapping mechanism that projects both the foreground (human) and background models into a unified representation space. This simple yet effective design explicitly addresses the fundamental challenge of integrating models with different initialization strategies, architectural designs, and optimization objectives. The key insight is that without proper alignment, these separately modeled components, despite being concatenated during rendering, lack a unified representation space, leading to spatial inconsistencies, floating artifacts, and incorrect occlusions, particularly at human-scene interaction boundaries.

However, establishing explicit communication between these components is challenging because both Gaussian fields contain millions of Gaussian primitives with fundamentally different spatial structures. To address this, we introduce a shared non-linear transformation function that operates across both sets of Gaussian fields. This shared design maximizes computational efficiency by avoiding exhaustive pairwise interactions between all foreground and background primitives. Instead, it utilizes learnable projections along the attribute dimension to map both Gaussian fields into a unified representation space. Specifically, we apply separate transformations for each Gaussian attribute, including position, color, opacity, rotation, and scale, which enabling attribute-specific alignment. This per-attribute processing ensures that each property is aligned according to its distinct semantic role in

Wenqing Wang, Josef Kittler are with the Centre for Vision, Speech and Signal Processing (CVSSP), University of Surrey. (e-mail: wenqing.wang@surrey.ac.uk, j.kittler@surrey.ac.uk). Haosen Yang and Xiatian Zhu are with Centre for Vision, Speech and Signal Processing (CVSSP) and People-Centred Artificial Intelligence (PAI), University of Surrey. (e-mail: h.yang@surrey.ac.uk, xiatian.zhu@surrey.ac.uk)

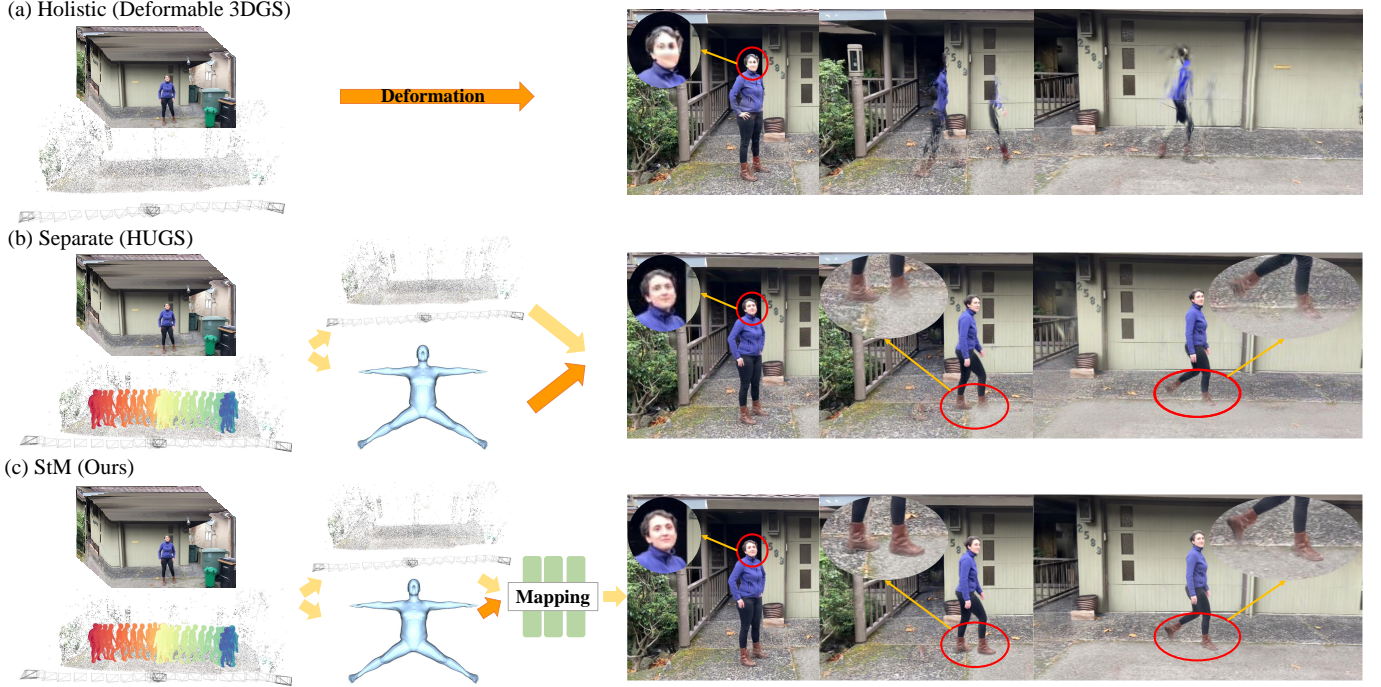


Fig. 1. Learning from a limited monocular video of a human moving around the scene, existing approaches face several challenges: (a) Holistic 4D reconstruction methods [1] struggle to maintain the integrity of the avatar. (b) Separate-based methods [2] suffer from unexpected occlusions and floating artifacts in the regions where the background and the avatar interact. (c) In contrast, our Separate-then-Map (StM) strategy achieves more accurate and complete reconstruction by mapping different model representations to a unified space.

the rendering process.

This work makes three contributions: (1) We systematically identify and investigate a previously overlooked problem of missing information communicate between separately modeled foreground and background in human-centric 4D scene reconstruction. (2) We propose StM, which introduces a shared information mapping mechanism to project separately initialized, designed, and optimized components into a unified space, ensuring both computational efficiency and spatial coherence. (3) Extensive experiments on monocular video datasets demonstrate that StM significantly outperforms existing state-of-the-art methods in both visual quality and rendering accuracy.

II. RELATED WORK

A. 4D novel view synthesis and reconstruction

4D Novel view synthesis and reconstruction provides a general and holistic solution for reconstructing dynamic objects and scene contents. Recent methods have introduced various dynamic representations such as dynamic NeRF [19, 20, 21], dynamic triplane [22, 23], and dynamic Gaussian Splatting [1, 12, 24, 25, 26], enabling high-quality rendering from both calibrated multi-view and uncalibrated monocular RGB video inputs. Especially, point-based explicit representations (e.g., Gaussian Splatting) have achieved state-of-the-art rendering quality while maintaining real-time inference and training efficiency. Dynamic 3DGS [25] optimize the position and shape of each Gaussian kernel frame-by-frame, while Deformable 3DGS [1] and 4DGS [12] introduce time-dependent deformation networks to deform a canonical 3D Gaussian

into each frame. [24, 27] expand 3D Gaussian primitives to 4D by incorporating temporal properties. Despite their effectiveness, these approaches are most suitable for scenes with slow-moving objects [19, 21]. Furthermore, they treat the entire scene holistically without integrating statistical models for regularization. This limitation is particularly significant in human-centric scenarios, where prior body models such as SMPL [17] can provide valuable structural constraints. Therefore, our method incorporates human prior knowledge to better handle large motions.

B. Human avatars reconstruction and animation

Human avatars reconstruction and animation from visual observations remains a challenging task. Traditional methods relying on explicit, predefined parametric mesh topologies [17, 28, 29, 30] often struggle to capture personalized appearance details [31]. With the advancements in neural representations [32, 33], recent studies [3, 4, 5, 6, 8, 34, 35, 36, 37, 38, 39, 40, 41, 42, 43] have integrated parametric template models [17, 28, 29, 30] to reconstruct dynamic human avatars. These hybrid approaches not only capture fine-grained, personalized details but also enable the animation of reconstructed avatars through simple pose guidance. However, the aforementioned methods primarily focus on reconstructing and animating avatars in isolation, disregarding the surrounding environment. In real-world scenarios, where visual inputs contain rich contextual information, it is essential to reconstruct both the avatar and its environment to achieve a more comprehensive understanding of the scene. Our method aims to reconstruct and animate human avatars within their captured environments.

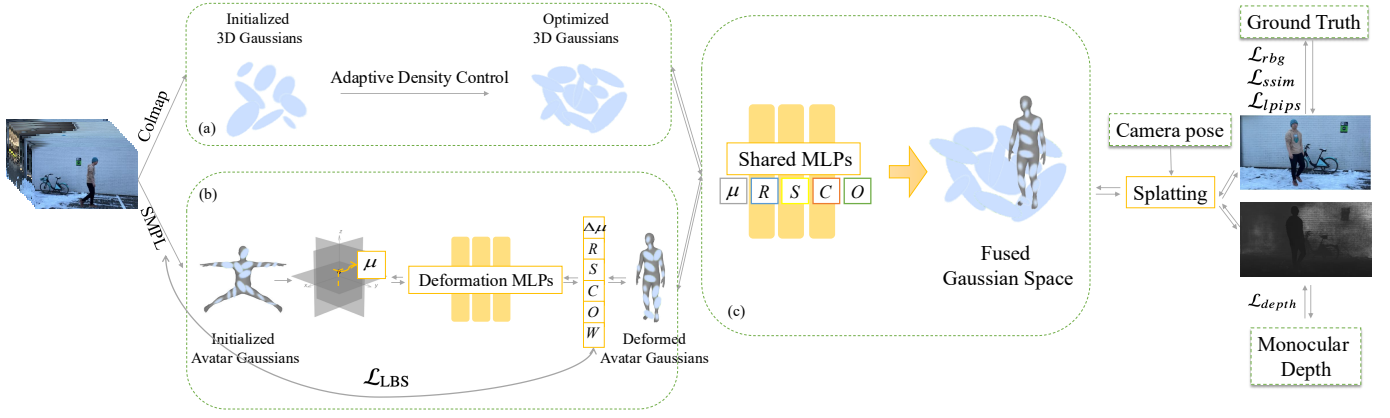


Fig. 2. **Overview of Separate-then-Map (StM):** Given an input video sequence, we first initialize the point clouds for the scene and avatar Gaussians using Colmap predictions and SMPL vertex points. This decoupled design is as follows: (a) a 3D Gaussian Splatting (3DGS) model represents the background scene, (b) a deformable 3D Gaussian avatar model driven by linear blend skinning (LBS) to represent the foreground human, with the parameters including position offset $\Delta\mu$, rotation R , scale S , spherical harmonics (SH) coefficients C , opacity O , and LBS weight W , all predicted from the position triplane feature μ ; (c) A information mapping process is then employed to project the scene model and the avatar model into a consistent space. During training, the rendered images and depth maps are used to compute the loss against the ground truth images and monocular estimated depth maps.

C. Dynamic human reconstruction and animation in context

Dynamic human reconstruction and animation in context is becoming increasingly important as virtual avatars interact more closely with their surrounding environments. Recent methods [2, 13, 14] have explored detaching the avatar from the background using separate neural fields while incorporating strong human priors to simplify the overall reconstruction process. Specifically, Neuman [13] trains two NeRF models [32] - the scene NeRF and the human NeRF successively - encoding the human’s appearance and geometry separately from the background. Similarly, Vid2Avatar [14] models the foreground human and background scene using two separate neural fields without relying on external segmentation modules. Utilizing 3D Gaussian Splatting, HUGS [2] defines two sets of Gaussian fields with distinct predefined properties, which are subsequently concatenated and rendered together during splatting and optimization. Separating the background and avatar is an efficient strategy for reconstructing complex human motion while maintaining photorealistic rendering. However, existing methods do not consider how to project and recombine different model representations, potentially leading to inconsistencies in integration. To overcome this limitation, our method maps the representation spaces of the two models into a unified one during training, enabling more coherent and realistic reconstructions.

III. METHOD

Problem definition Given a monocular video captured by a moving camera that shows a human moving through a natural background, our goal is to learn a 4D model capable of rendering the human from novel viewpoints and animating the human in novel poses, both within the observed scene and in new scenes. Monocular video is typically short, providing limited views and poses of the human while continuously moving around the scene. This setup introduces challenges due to sparse views, significant body displacement, and variation in both the scene and the human over time.

Model architecture To address this challenging human-centric 4D scene reconstruction problem, we propose StM strategy. Specifically, we adopt a decoupling design for background and foreground, where the scene and human are parameterized independently with specialized representation models. After separately modeling, we introduce a shared information mapping module that project information from both Gaussian models into a shared space. This transformation effectively mitigates issues related to separate initialization, and distinct model structures and optimization processes. Our overall architecture, illustrated in Figure 2, consists of: (a) a scene model, (b) a deformable human avatar model, and (c) a shared information mapping module.

A. Scene model

We adopt 3DGS [33] for scene representation due to its effective balance between efficiency and accuracy. First, camera poses and the initial point cloud are estimated from a given video sequence using Colmap [44, 45]. The point cloud is initialized as a set of 3D Gaussian primitives, denoted \mathcal{G}_b . Each Gaussian primitive G_k is defined by its position (mean) μ , covariance matrix Σ and opacity o :

$$G_k = \exp(-\frac{1}{2}(\mathbf{x} - \mu)^T \Sigma^{-1}(\mathbf{x} - \mu)). \quad (1)$$

The covariance matrix Σ factorized into a scaling matrix S and a rotation matrix R : $\Sigma = RSS^T R^T$.

For rendering, the 3D Gaussians are projected onto the 2D image plane to form 2D Gaussians, denoted G_k^{2D} . For any given camera pose P_i , an image can be rendered by splatting and alpha blending N sorted Gaussians visible in this view:

$$I' = R(\mathcal{G}_b, P_i) = \sum_{k=1}^N o_k G_k^{2D} c_k(P_i) \prod_{j=1}^{k-1} (1 - o_j G_j^{2D}), \quad (2)$$

where R represents the differentiable Gaussian rasterizer, c_k is the view-dependent color of the k -th Gaussian, I' denotes the rendered image, which can be used to calculate photometric loss with ground truth images.

B. Human avatar deformation model

Combine parametric human prior model, such as SMPL [17], with implicit or explicit neural rendering enables more complete reconstruction and novel pose animation, as demonstrated by several works [3, 4, 13, 46]. Therefore we utilize a Linear Blend Skinning (LBS)-driven deformable 3D Gaussians \mathcal{G}_a [2] to represent the human avatar. The estimated SMPL parameters β and θ for each frame are used to regularize body shapes and poses [17, 47].

Specifically, for each Gaussian kernel, taken its position triplane feature as input, which is passed through three MLP deformation modules to predict Gaussian point's position offset, color, opacity, rotation, scale and LBS weights. The movement of each Gaussian primitive from the canonical position p^c to posed position p^θ is driven by the optimized LBS weights using forward skinning:

$$p^\theta = \sum_{k=1}^K w_k (\mathbf{B}_k(\mathbf{J}, \theta) p^c + \mathbf{b}_k(\mathbf{J}, \theta, \beta)), \quad (3)$$

where \mathbf{J} includes K joint locations, $\mathbf{B}_k(\mathbf{J}, \theta)$ and $\mathbf{b}_k(\mathbf{J}, \theta, \beta)$ are the transformation matrix and translation vector of joint k respectively, w_k is the linear blend weight for this Gaussian primitive.

C. Human and Scene shared information mapping

The separate modeling of the scene and human avatar have suboptimal initialization and employ different model design and optimization strategies, although they are concatenate together for rendering and gradient back-propagation in the previous method [2], still no direct correspondence or pairing relationship between scene and avatar Gaussian primitives, which will cause conflict and geometry inconsistency, displaying outside as floating artifacts and foreground occlusions. To map separately modeled components into an unified space, we introduce a shared information mapping module for per-attribute.

Given the presence of millions of Gaussian primitives, directly modeling cross-interactions between the scene and human avatar would be computationally prohibitive. To address this challenge, we introduce a shared non-linear transformation function, specifically a residual MLP that maps each Gaussian primitive, whether belonging to the scene or the human avatar, into a unified integration space. This approach enables efficient and structured information exchange while maintaining computational feasibility. Furthermore, each Gaussian primitive is associated with a set of attributes, including position, opacity, color, scale, and rotation. These attributes, each carrying distinct semantic significance, are freely optimized and require individualized processing. Taking these factors into account, we extend transformation function to each Gaussian attributes, which enables a more structured and efficient projection between the background scene and the human avatar.

Specifically, for each attribute i we introduce the shared transformation function ϕ_i (e.g., a shared residual MLP) as:

$$\mathcal{G}_a^{i'} = \mathcal{G}_a^i + \phi_i(\mathcal{G}_a^i), \quad \mathcal{G}_b^{i'} = \mathcal{G}_b^i + \phi_i(\mathcal{G}_b^i), \quad (4)$$

where \mathcal{G}_a^i and \mathcal{G}_b^i denote the i -th Gaussian attribute of the background (\mathcal{G}_b) and avatar (\mathcal{G}_a) models. After being aligned,

the two models can be simply concatenated and fed into the rendering process to produce the final images.

D. Discussion

To demonstrate that our shared mapping module effectively exchanges information beyond a residual function, we compare our method with an alternative approach that applies separate residual MLPs for each Gaussian fields per-attribute. Specifically, while our method uses a shared-weight MLP per attribute type that processes primitives from both background and avatar fields (enabling cross-model information flow through weight sharing), the separate baseline uses independent MLPs with distinct weights for each field—one for background and one for avatar—resulting in a lack of information exchange between the two components. As shown in Table IV (b) and (c), this separate approach leads to a significant performance drop compared to our shared method, validating that the shared-weight architecture is crucial for learning a unified transformation that properly aligns both sets of Gaussian primitives into a coherent representation space.

Utilizing a shared-weight MLP along the attribute dimension of each primitive, rather than across all primitives, has similar practice in PointNet [48, 49]. However, PointNet emphasizes the permutation-invariant processing of unordered point clouds through symmetric aggregation functions, whereas our approach focuses on learning a nonlinear transformation that projects both sets of separately initialized and optimized Gaussian primitives into a unified representation space. The key distinction is that our shared weights enable bidirectional information flow between foreground and avatar components during training: gradients from both fields jointly optimize the same transformation parameters, forcing the network to discover a common alignment strategy that works coherently for both components, thereby enabling effective integration of independently modeled human avatars and background scenes.

E. Mapping network details

We present a detailed overview of our shared information mapping module. Specifically, we adopts non-linear lightweight residual MLPs for each attribute, including position, SH, opacity, scale, rotation, defined as:

$$\phi_i = \text{Linear}_2(\text{ReLU}(\text{Linear}_1(\mathcal{G}^i))) \quad (5)$$

where \mathcal{G}^i is the i -th attribute of Gaussian models. The input dimension corresponds to the dimension of each attribute, while the hidden dimension of ϕ_i is set to 64.

F. Model training

Our model is trained end to end, with the learnable parameters distributed in the background scene \mathcal{G}_b and avatar Gaussians \mathcal{G}_a models, the feature triplane, deformation modules, as well as our information mapping module. Specifically, we adopt standard image-based losses between rendered and ground truth images: \mathcal{L}_{rgb} for RGB similarity, \mathcal{L}_{ssim} based on the SSIM metric [50], and $\mathcal{L}_{lpi ps}$ for perceptual similarity [51]. Following HUGS [2],

TABLE I

COMPARING THE NOVEL VIEW SYNTHESIS RESULTS OF THE WHOLE *scenes* ON NEUMAN [13] DATASET. THE FRONT PART IS HOLISTIC 4D SCENE RECONSTRUCTION METHODS, AND THE SECOND PART IS SEPARATE MODELED RECONSTRUCTION METHODS. AND THE LAST PART IS OUR PROPOSED StM RESULTS. NOTE, 4DGS FAILED TO CONVERGE ON THE LAB SCENE, RESULTING IN NO RESULTS. HUGS* IS OUR RE-IMPLEMENTATION TRAINED FOR 20,000 ITERATIONS COMPARED WITH ORIGINAL 15,000 ITERATIONS.

	Seattle			Citron			Parking			Bike			Jogging			Lab		
	PSNR↑	SSIM↑	LPIPS↓	PSNR↑	SSIM↑	LPIPS↓	PSNR↑	SSIM↑	LPIPS↓	PSNR↑	SSIM↑	LPIPS↓	PSNR↑	SSIM↑	LPIPS↓	PSNR↑	SSIM↑	LPIPS↓
NeRF-T [20]	21.84	0.69	0.37	12.33	0.49	0.65	21.98	0.69	0.46	21.16	0.71	0.36	20.63	0.53	0.49	20.52	0.75	0.39
HyperNeRF [21]	16.43	0.43	0.40	16.81	0.41	0.56	16.04	0.38	0.62	17.64	0.42	0.43	18.52	0.39	0.52	16.75	0.51	0.23
D3DGS [1]	25.02	0.91	0.13	19.68	0.78	0.25	21.67	0.88	0.23	19.78	0.85	0.16	20.60	0.82	0.24	19.10	0.88	0.18
4DGS [12]	23.23	0.87	0.17	19.19	0.77	0.30	21.85	0.75	0.42	21.85	0.87	0.16	22.02	0.80	0.27	-	-	-
Vid2Avatar [14]	17.41	0.56	0.60	14.32	0.62	0.65	21.56	0.69	0.50	14.86	0.51	0.69	15.04	0.41	0.70	13.96	0.60	0.68
NeuMan [13]	23.99	0.78	0.26	24.63	0.81	0.26	25.43	0.80	0.31	25.55	0.83	0.23	22.70	0.68	0.32	24.96	0.86	0.21
HUGS [2]	25.94	0.85	0.13	25.54	0.86	0.15	26.86	0.85	0.22	25.46	0.84	0.13	23.75	0.78	0.22	26.00	0.92	0.09
HUGS* [2]	26.26	0.85	0.10	25.68	0.86	0.09	26.69	0.84	0.14	25.94	0.85	0.09	23.71	0.77	0.18	26.09	0.92	0.07
StM	27.60	0.91	0.06	26.44	0.87	0.09	27.49	0.88	0.10	26.75	0.88	0.07	24.57	0.82	0.15	26.60	0.92	0.06

TABLE II

COMPARING THE NOVEL VIEW SYNTHESIS RESULTS OF THE *HUMAN* REGION ON NEUMAN [13] DATASET.

	Seattle			Citron			Parking			Bike			Jogging			Lab		
	PSNR ↑	SSIM ↑	LPIPS ↓	PSNR ↑	SSIM ↑	LPIPS ↓	PSNR ↑	SSIM ↑	LPIPS ↓	PSNR ↑	SSIM ↑	LPIPS ↓	PSNR ↑	SSIM ↑	LPIPS ↓	PSNR ↑	SSIM ↑	LPIPS ↓
Vid2Avatar [14]	16.90	0.51	0.27	15.96	0.59	0.28	18.51	0.65	0.26	12.44	0.39	0.54	16.36	0.46	0.30	15.99	0.62	0.34
NeuMan [13]	18.42	0.58	0.20	18.39	0.64	0.19	17.66	0.66	0.24	19.05	0.66	0.21	17.57	0.54	0.29	18.76	0.73	0.23
HUGS [2]	19.06	0.67	0.15	19.16	0.71	0.16	19.44	0.73	0.17	19.48	0.67	0.18	17.45	0.59	0.27	18.79	0.76	0.18
HUGS* [2]	18.80	0.64	0.13	18.99	0.70	0.13	19.14	0.72	0.15	19.82	0.67	0.14	17.25	0.58	0.23	18.88	0.76	0.15
StM	19.93	0.71	0.12	20.20	0.71	0.12	19.80	0.73	0.14	20.41	0.70	0.14	18.28	0.62	0.21	19.73	0.77	0.14

we apply image-level losses (\mathcal{L}_{rbg}^a , \mathcal{L}_{ssim}^a , \mathcal{L}_{lpiPs}^a) specifically to the avatar Gaussian rendering.

Additionally, each avatar Gaussian primitive’s LBS weights are regularized by \mathcal{L}_{lbs} [2, 40], ensuring they match the distance-weighted average of the k nearest mesh vertices weights estimated by SMPL [17]. Specifically, we employ an ℓ_2 loss to regularize the LBS weights \mathbf{W} of the Gaussian points, ensuring they closely align with the LBS weights of nearby SMPL vertices. For each individual Gaussian \mathbf{p}_i , we retrieve its $k = 6$ nearest vertices on the SMPL mesh. A distance-weighted average of the LBS weights of these vertices is computed to obtain $\hat{\mathbf{W}}$. And the loss is

$$\mathcal{L}_{LBS} = \|\mathbf{W} - \hat{\mathbf{W}}\|_F^2. \quad (6)$$

To further improve the global coherent representation, we add a depth regularization loss \mathcal{L}_{depth} . To handle scale ambiguity in the monocular estimated depth map, we apply a *pearson* correlation loss [52], that enforces only the linear relationship between the monocular estimated depth \hat{D}_{est} and the rendered depth \hat{D}_{ras} rather than their absolute values, as described by the following function:

$$\mathcal{L}_{depth} = \text{Corr}(\hat{D}_{ras}, \hat{D}_{est}) = \frac{\text{Cov}(\hat{D}_{ras}, \hat{D}_{est})}{\sqrt{\text{Var}(\hat{D}_{ras}) \text{Var}(\hat{D}_{est})}} \quad (7)$$

This relaxed constraint enables the alignment of depth structures without being obstructed by inconsistencies in absolute depth values.

As we demonstrated in Sec IV-D, simply increasing depth regularization is insufficient to solve our main proposed problem, as single-view depth estimation remains imprecise and noise, particularly in regions where the human subject interacts with the environment.

The overall objective loss function is therefore:

$$\begin{aligned} \mathcal{L} = & \lambda_{rbg} \mathcal{L}_{rbg} + \lambda_{ssim} \mathcal{L}_{ssim} + \lambda_{lpiPs} \mathcal{L}_{lpiPs} \\ & + \lambda_{rbg} \mathcal{L}_{rbg}^a + \lambda_{ssim} \mathcal{L}_{ssim}^a + \lambda_{lpiPs} \mathcal{L}_{lpiPs}^a \\ & + \lambda_{lbs} \mathcal{L}_{lbs} + \lambda_{depth} \mathcal{L}_{depth}, \end{aligned} \quad (8)$$

where we consistently set all hyperparameters as follows: $\lambda_{rbg} = 0.8$, $\lambda_{ssim} = 0.2$, $\lambda_{lpiPs} = 1.0$, $\lambda_{lbs} = 100$, $\lambda_{depth} = 0.02$ across all the scenes.

G. Novel view, novel pose and novel scene synthesis

The background scene and human avatar models provide a rich environment for creating a diverse range of human-centric scenarios. Novel view synthesis for both the original scene and the human avatar is naturally supported. To compose a specific scenario, we begin by selecting a background scene—either the original or a new one—then set the motion sequence and relative relationship of the avatar within the scene. The human avatar is flexible animated by motion sequences with the help of SMPL [17] model. The final scenario is constructed by positioning the human avatar model according to its scene coordinates and integrating both models in their original form (Gaussian primitives). Standard rasterization-based rendering is then applied to generate a specific view of the whole scenario.

IV. EXPERIMENTS

A. Experimental settings

Dataset We use *NeuMan* dataset [13] with six video sequences, named Seattle, Citron, Parking, Bike, Jogging, and Lab, taken from in-the-wild environments using a moving mobile phone camera. We follow the official training and testing splits [13] to facilitate fair comparison with existing competitors.

Evaluation metrics. We consider three image quality metrics: including the peak signal-to-noise ratio (PSNR), structural

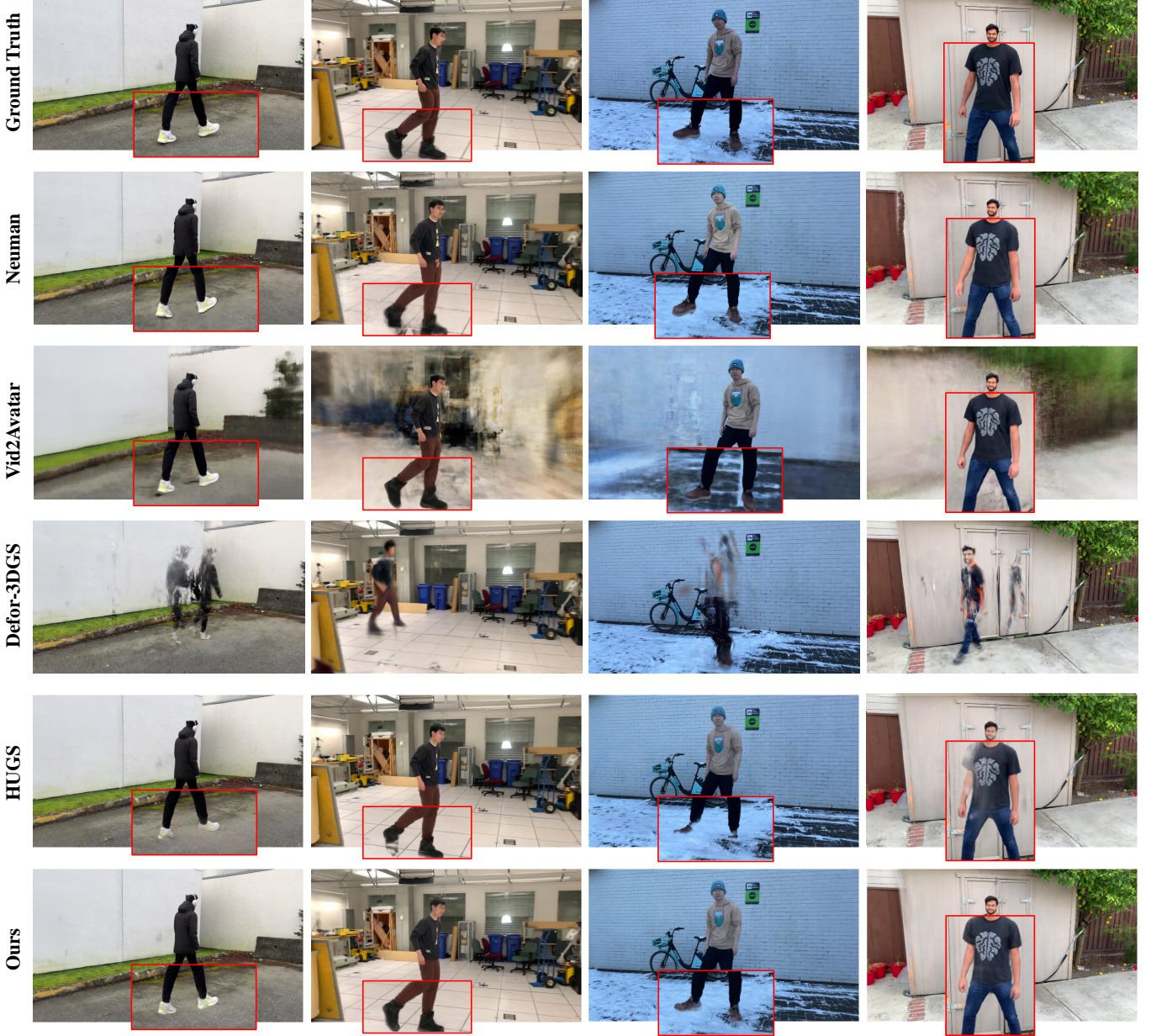


Fig. 3. Qualitative comparison for novel view synthesis comparing our StM with HUGS [2], D3DGS [1], Vid2Avatar [14], and Neuman [13]. The zoomed-in regions (red box) highlight the difference.

similarity index measure (SSIM) [50], and the learned perceptual image patch similarity (LPIPS) [51], which are broadly recognized standards in the field.

Implementation details. We employ the Adam optimizer [53] for training. To optimize the position of Avatar Gaussians and Scene Gaussians, we initialize the learning rate to 1.6^{-4} and terminate to 1.6^{-6} , coupled with an exponential learning rate decay. For the information mapping module, we more heavily initialize the learning rate to 10^{-3} and terminate to 10^{-5} , also using an exponential schedule. During the optimization process, we clone, split, and prune scene Gaussian field every 100 iterations [33], and these operations are applied to the avatar Gaussian fields every 600 iterations [2]. The entire optimization process runs for 20,000 iterations on a single NVIDIA RTX 3090

GPU. All presented results for GS-based methods are averaged over three runs with different seeds.

B. Quantitative analysis

Novel view synthesis evaluation. We compare the novel view synthesis results by our method and existing state of the art alternatives in the categories of NeRF-based whole dynamic scene reconstruction methods: NeRF-T [20], HyperNeRF [21]; NeRF-based detached modeling methods: Neuman [13], Vid2Avatar [14]; Gaussian-based whole dynamic scene reconstruction methods: Deformable 3D Gaussian (D3DGS) [1], 4DGS [12]; and Gaussian-based detached method: HUGS [2].

The novel view synthesis results for the whole scenes are presented in Table I. We highlight several key observations: (1) By modeling the whole scene using a single representation model, previous methods all face challenges for novel view rendering, regardless using either NeRF (NeRF-T [20], HyperNeRF [21]) or Gaussian splatting (4DGS [12], D3DGS [1]). In particular, HyperNeRF is the worst of dealing with drastically dynamic scenes with humans, likely due to its reliance of dense multi-view images. (2) Although a couple of methods (Neuman [13] and Vid2Avatar [14]) learn the background and human avatar separately, a limited performance gain is achieved. As they suffer from inferior background optimization (Vid2Avatar [14]) or the challenge of modeling photorealistic the human body parts (Neuman [13]). (3) By effectively addressing these challenges, HUGS [2] significantly enhances the quality of novel view rendering. This improvement is primarily attributed to the introduction of the human parametric model-aware 3DGS-based representation, which enables end-to-end optimization. However, this approach overlooks the integration issue between the separately modeled background and foreground. (4) By tackling this problem and increasing the shared information mapping module, our StM strategy further enhances the render-

ing performance substantially.

Human-scene interaction region evaluation. We further focus on the quality of the human-scene interaction region by cropping the human using a human detector [54] from the entire testing images. This evaluation specifically targets the challenging boundary areas where avatar and background meet—regions most prone to floating artifacts, occlusion errors, and blending inconsistencies. As shown in Table II, we observe that StM also achieves a significant performance improvement over the competitors, indicating that our shared information mapping mechanism successfully mitigates boundary artifacts and ensures spatial coherence in the critical interaction regions.

Comparison with avatar-only reconstruction methods. To further validate our approach, we compare against recent avatar-only reconstruction methods that focus solely on human modeling without explicit scene integration: GaussianAvatar [5] and GauHuman [4]. Unlike the interaction region evaluation above (which crops humans from full scene reconstructions), this comparison evaluates methods that only model avatars, typically using foreground masks to isolate humans during training. As shown in Table III, even when evaluating only the avatar, our method substantially outperforms these avatar-specialized



Fig. 4. Qualitative evaluation for novel pose synthesis and novel scene composition. Our method generates high-quality results that maintain the fine details and integrity of the avatar, and showing reduced floating artifacts in the background scene.

TABLE III
AVATAR-ONLY COMPARISON ON NEUMAN DATASET

Model	PSNR \uparrow	SSIM \uparrow	LPIPS \downarrow
GaussianAvatar	25.10	0.96	0.040
GauHuman	22.12	0.93	0.046
Ours	30.42	0.97	0.022

approaches. This significant gap demonstrates that modeling the human and scene jointly—rather than in isolation—provides stronger constraints and better handles the challenging aspects of monocular reconstruction such as limited viewpoints and complex human-scene interactions. These results validate our motivation that holistic scene modeling with proper integration mechanisms is essential for high-quality human-centric reconstruction.

Moreover, our StM strategy only increases MLP layers with a limited number of parameters, therefore, the additional computational time introduced is minimal. Specifically, it increases by only 0.001 seconds per iteration, resulting in an overall increase of 20 seconds per scene. This demonstrates that our method achieves significant quality improvements with negligible additional cost.

C. Qualitative analysis

Novel view synthesis evaluation. In Figure 3 and Figure 8, we show the qualitative results compared with Neuman [13], Vid2Avatar [14], D3DGS [1], HUGS [2]. We make the following observations: (1) Without treating the background scene and foreground human avatar separately, D3DGS [1] even fails to model the intact human body. This is plausibly due to not utilizing parametric human prior. (2) By separately modeling the human from the background scene, Vid2Avatar [14] can achieve whole body rendering, but degrading the quality of the background, due to their foreground focused modeling design. (3) While Neuman [13] improves background modeling, it still faces issues like stiff and unnatural effects. A plausible reason is due to the intrinsic difficulty of implicit representation model (NeRF) in dealing with structural objects like human. (4) To leverage explicit representation model like HUGS [2] achieves more fluid human avatar models along with good quality of background scene, thanks to its combination with learnable parametric mesh representation. However, they still doesn't work well especially where avatar interact with the background, such as rendering mixture of background and human from region to region, the floating effect, blurring boundary and artifacts around the human avatar. This indicates that the foreground and background models are not belong to same representation space during the rendering process, as they are parameterized individually and optimized with different strategies without effective interaction. (5) By introducing the shared information mapping for per-attribute appropriately, our StM strategy addresses this issue effectively and efficiently, as demonstrated by significantly improved novel view synthesis with finer details, reduced ghost effects, more complete human body, and better photo realism.

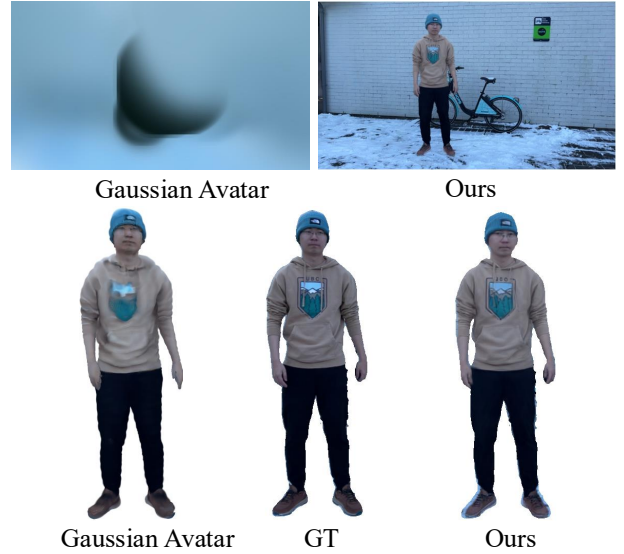


Fig. 5. GaussianAvatar cannot reconstruct the entire scene, also rendering inferior avatar.

Comparison with avatar-only reconstruction methods. To further validate our holistic scene modeling approach, we compare against recent avatar-only reconstruction methods that focus solely on human modeling: GaussianAvatar [5]. As shown in Figure 5, GaussianAvatar cannot reconstruct the entire scene and produces inferior avatar quality compared to our method. This validates our core motivation that holistic scene modeling with proper integration mechanisms is essential for high-quality human-centric reconstruction.

Novel poses and novel scene evaluation. We present a comparison of novel pose synthesis and novel scene composition between StM and HUGS [2]. As shown in Figure 4, HUGS exhibits several limitations: undesired foggy and ghosting effects in the rendered avatars (particularly visible in the torso and limbs), incomplete reconstruction of body parts such as legs and feet (highlighted in red boxes), and background contamination with floating artifacts near avatar-scene boundaries. In contrast, our StM renders the human avatar with significantly improved completeness, sharper boundaries, and cleaner separation from the background. Importantly, these advantages extend to the more challenging case of novel scene composition (bottom two rows), where avatars are transferred to entirely new environments. While HUGS struggles with increased blurriness and incomplete rendering in novel scenes, our method maintains avatar fidelity and generates more photorealistic compositions. This demonstrates that our shared information mapping mechanism learns more robust and generalizable avatar representations that reliably compose with novel backgrounds, validating the effectiveness of our approach across the full spectrum of human-centric 4D reconstruction tasks.

D. Ablation study

We conduct comprehensive ablation experiments to validate the effectiveness of each component in our method. All experiments are performed on the NeuMan dataset following the same protocol as our main evaluation. Table IV presents

TABLE IV

ABLATION STUDY OF (A) IMPACT OF ESTIMATED DEPTH REGULARIZATION; (B) IMPACT OF OUR PROPOSED SHARED INFORMATION MAPPING MODULE (WITHOUT DEPTH); (C) RESULTS FOR SEPARATE MLPs INSTEAD OF SHARED MLPs; (D)-(F) EFFECTS OF PER GAUSSIAN ATTRIBUTE MAPPING; (G) FULL MODEL (SHARED MAPPING WITH DEPTH REGULARIZATION).

	Seattle			Citron			Parking			Bike			Jogging			Lab		
	PSNR \uparrow	SSIM \uparrow	LPIPS \downarrow	PSNR \uparrow	SSIM \uparrow	LPIPS \downarrow	PSNR \uparrow	SSIM \uparrow	LPIPS \downarrow	PSNR \uparrow	SSIM \uparrow	LPIPS \downarrow	PSNR \uparrow	SSIM \uparrow	LPIPS \downarrow	PSNR \uparrow	SSIM \uparrow	LPIPS \downarrow
(a) w/ depth	26.39	0.8504	0.0964	26.06	0.8634	0.0892	26.99	0.8447	0.1373	26.10	0.8527	0.0941	23.75	0.7677	0.1861	26.17	0.9171	0.0689
(b) w/ shared mapping	27.44	0.9068	0.0650	26.26	0.8661	0.0879	27.21	0.8766	0.1087	26.38	0.8799	0.0767	24.51	0.8206	0.1521	26.51	0.9215	0.0648
(c) separate MLPs	26.63	0.8721	0.0794	25.85	0.8585	0.0926	26.12	0.8586	0.1252	25.63	0.8374	0.1084	24.00	0.7988	0.1706	25.24	0.8863	0.1181
(d) w/o position	27.58	0.9096	0.0633	26.37	0.8589	0.0883	27.24	0.8643	0.1200	26.58	0.8819	0.0737	24.34	0.8137	0.1571	26.44	0.9149	0.0734
(e) w/o opacity	27.01	0.8909	0.0734	24.43	0.8499	0.1058	26.95	0.8601	0.1195	26.20	0.8781	0.0750	24.05	0.7995	0.1574	26.31	0.9143	0.0720
(f) w/o color	27.58	0.9094	0.0655	26.24	0.8581	0.0881	27.20	0.8623	0.1246	26.41	0.8789	0.0765	24.30	0.8091	0.1521	26.39	0.9145	0.0720
(g) Full	27.60	0.9097	0.0620	26.44	0.8674	0.0874	27.49	0.8771	0.1049	26.75	0.8836	0.0705	24.57	0.8226	0.1510	26.60	0.9225	0.0634

quantitative results: (a) evaluates depth regularization alone, (b) evaluates our shared mapping mechanism without depth, (c) compares against separate MLPs baseline, (d)-(f) ablate individual attribute mappings, and (g) shows our complete model with both shared mapping and depth regularization.

Effect of depth regularization. Depth regularization is a common approach to improving geometric consistency. As shown

in Table IV(a), incorporating monocular depth supervision does provide measurable benefits over the baseline HUGS. However, qualitative analysis reveals critical limitations. Figure 6(b) shows that depth supervision still produces semi-transparent regions and spatial inconsistencies at ground contacts, with residual avatar traces contaminating background regions. This occurs because monocular depth estimation suffers from scale

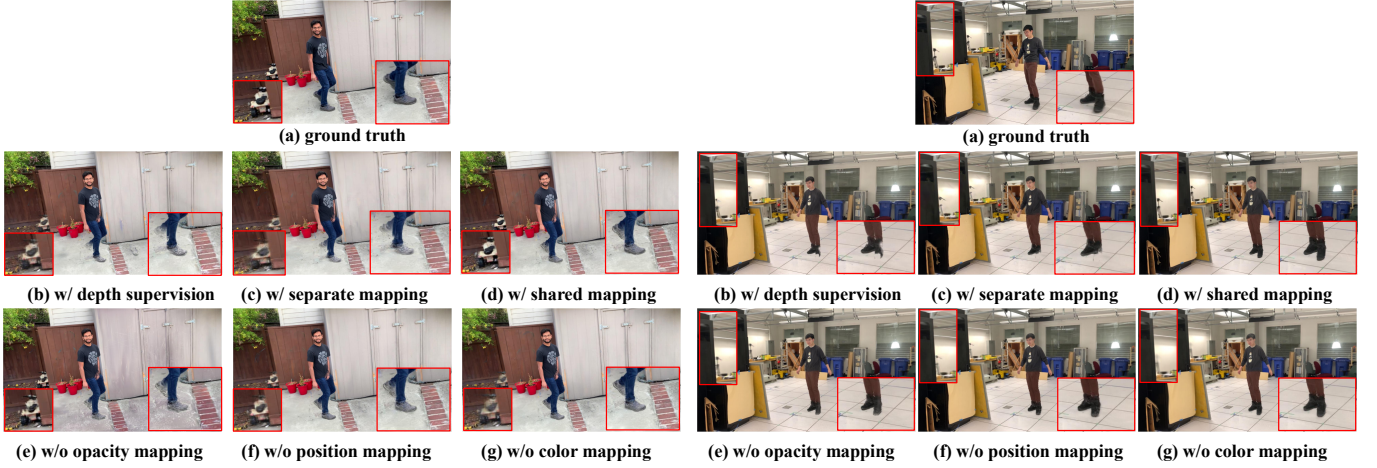


Fig. 6. Qualitative ablation study on mapping strategies and per-attribute alignment. (a) Ground truth. (b) Depth supervision improves over baseline but exhibits blur at boundaries. (c) Separate mapping per field produces semi-transparent regions and blurred boundaries. (d) Our shared-weight mapping achieves clean, well-defined integration. (e)-(g) Ablations removing individual attribute mappings: without opacity mapping (e), severe ghosting appears; without position mapping (f), floating artifacts emerge; without color mapping (g), slight boundary blur occurs. Red boxes highlight critical interaction regions.

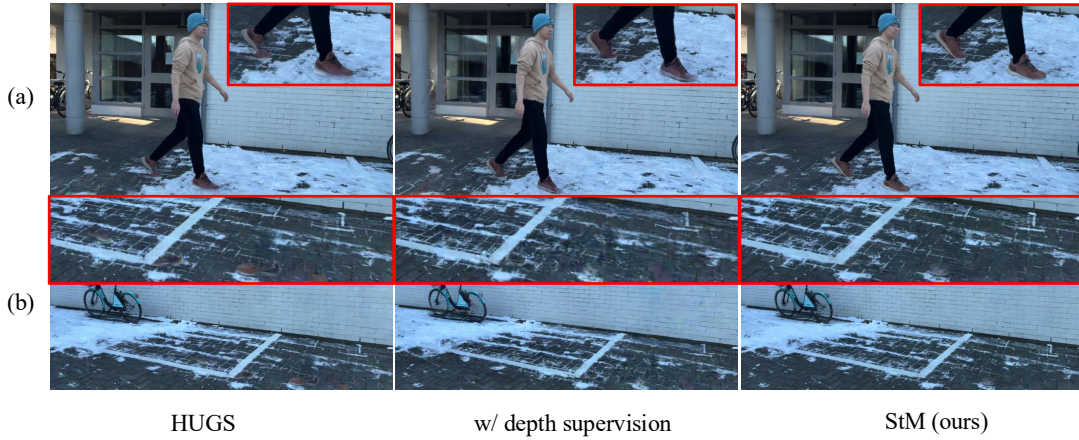


Fig. 7. Depth regularization analysis. (a) Full scene rendering: HUGS exhibits severe blur at human-scene boundaries (feet/ground contact, highlighted in red boxes). Depth supervision improves structure but still produces blurred boundaries compared to our method. (b) Background-only rendering: HUGS with depth supervision leaves visible avatar residue (ghostly imprints in red boxes) in the background, revealing that depth regularization cannot ensure clean foreground-background separation. Our method achieves sharp boundaries and artifact-free backgrounds.



Fig. 8. More qualitative comparison for novel view synthesis comparing our StM with HUGS [2], D3DGS [1], Vid2Avatar [14], and Neuman [13]. The zoomed-in regions (red box) highlight the difference.

ambiguity and noise, particularly in dynamic regions and occlusion boundaries. Figure 7 provides more comprehensive evidence through two views. In (a), full scene rendering shows HUGS with depth supervision still exhibits severe blur around the feet and lower body. The zoomed insets reveal the feet appear to “sink into” or “float above” the ground, indicating geometric constraints alone cannot resolve spatial inconsistencies without explicit model-to-model alignment. More revealing is (b), showing background-only rendering: HUGS with depth supervision clearly leaves visible residue artifacts—ghostly imprints of legs and feet persist in clean background regions (red box). This reveals depth regularization encourages geometric consistency within each model but does nothing to ensure clean separation between separately modeled avatar and background fields. The

monocular depth estimator cannot distinguish which primitives belong to foreground versus background in interaction regions, causing ambiguous assignments and contamination.

In contrast, our shared mapping explicitly addresses model-to-model correspondence by projecting both sets of primitives into unified space. As evident in both views, our method produces clean boundaries, eliminates residue artifacts, and maintains proper separation. These findings demonstrate that while depth provides weak geometric priors, it cannot substitute for explicit information exchange mechanisms. The noise and uncertainty in monocular depth estimation—especially in challenging in-the-wild captures—make it unreliable for interaction regions where integration quality matters most. Our alignment strategy, operating directly on Gaussian representations through

learned transformations, proves far more effective.

Effect of mapping strategy. To verify the effectiveness of our shared-weight mapping design, we compare against an alternative that applies separate residual MLPs for each Gaussian field per-attribute. To verify the effectiveness of our shared-weight mapping design, we compare our method (Table IV(b)) against an alternative that applies separate residual MLPs for each Gaussian field per-attribute (Table IV(c)). Our shared mapping substantially outperforms the separate way across all scenes (e.g., 27.44 vs. 26.63 PSNR on Seattle, 26.26 vs. 25.85 on Citron). Figure 6(c) and (d) illustrate this difference qualitatively: the separate strategy (c) produces semi-transparent regions and blurred boundaries at the avatar’s feet and lower body (red boxes), while our shared mapping (d) achieves clean, well-defined boundaries. This validates that shared-weight architecture is essential for coherent integration of separately modeled components. Further discussion on the information exchange mechanism is provided in Section III-D.

Effect of individual per-attribute mapping. We evaluate the necessity and contribution of each individual attributes mapping design. Here we examine three important ones: position, opacity, and color. Table IV(d)-(f) present ablations where we remove mapping for position, opacity, and color respectively. We observe that opacity mapping is the most critical component among all attributes, as expected since it directly controls visibility and the blending of overlapping Gaussians. As shown in Figure 6(e), without opacity alignment, severe ghosting effects and lighting inconsistencies appear at human-scene boundaries. The absence of color alignment (Figure 6(g)) results in slight background blurring, while missing position alignment (Figure 6(f)) introduces inconspicuous floating artifacts and occlusion in boundary regions. These results confirm that each attribute requires individualized alignment processing to achieve optimal integration quality.

V. LIMITATIONS

While our method demonstrates significant improvements in dynamic human-centric scene reconstruction, several challenges in monocular video reconstruction remain. First, our approach is sensitive to upstream estimations: inaccurate camera poses and imperfect SMPL fitting can propagate errors, causing misalignments and artifacts in complex interaction regions. Second, monocular setups suffer from limited observability—back-side views are severely under-constrained, resulting in incomplete geometry and texture hallucination in unobserved regions. Despite these limitations, our extensive evaluation demonstrates that StM advances the state-of-the-art in this challenging domain. Future work could explore multi-view priors, foundation models for robust pose and depth estimation, or stronger geometric constraints to further improve reconstruction quality.

VI. CONCLUSION

We introduce **StM**, a novel end-to-end strategy for dynamic human-centric scene reconstruction from monocular videos. Unlike prior approaches that either model scenes holistically or treat foreground and background as independent components with simple concatenation, we identify and address a critical

overlooked challenge: the lack of effective information exchange between separately modeled human avatars and background scenes. Our key contribution is a shared information mapping mechanism that projects separately designed components into a unified representation space, enabling coherent integration while maintaining computational efficiency. By applying lightweight residual MLPs to each Gaussian attribute, our approach achieves optimal scene modeling without exhaustive pairwise interactions between millions of primitives. Extensive experiments demonstrate that our method significantly outperforms state-of-the-art alternatives across novel view synthesis, novel pose synthesis, and novel scene composition. Qualitative results validate that StM effectively mitigates floating artifacts, occlusion issues, and boundary inconsistencies at challenging human-scene interaction regions. Our work establishes a foundation for integrated human-environment modeling with applications in AR/VR and digital human animation.

REFERENCES

- [1] Z. Yang, X. Gao, W. Zhou, S. Jiao, Y. Zhang, and X. Jin, “Deformable 3d gaussians for high-fidelity monocular dynamic scene reconstruction,” *arXiv preprint arXiv:2309.13101*, 2023.
- [2] M. Kocabas, J.-H. R. Chang, J. Gabriel, O. Tuzel, and A. Ranjan, “Hugs: Human gaussian splats,” in *Proceedings of the IEEE/CVF conference on computer vision and pattern recognition*, 2024, pp. 505–515.
- [3] C.-Y. Weng, B. Curless, P. P. Srinivasan, J. T. Barron, and I. Kemelmacher-Shlizerman, “Humannerf: Free-viewpoint rendering of moving people from monocular video,” in *Proceedings of the IEEE/CVF conference on computer vision and pattern recognition*, 2022, pp. 16 210–16 220.
- [4] S. Hu, T. Hu, and Z. Liu, “Gauhuman: Articulated gaussian splatting from monocular human videos,” in *Proceedings of the IEEE/CVF conference on computer vision and pattern recognition*, 2024, pp. 20 418–20 431.
- [5] L. Hu, H. Zhang, Y. Zhang, B. Zhou, B. Liu, S. Zhang, and L. Nie, “Gaussianavatar: Towards realistic human avatar modeling from a single video via animatable 3d gaussians,” in *Proceedings of the IEEE/CVF conference on computer vision and pattern recognition*, 2024, pp. 634–644.
- [6] G. Moon, T. Shiratori, and S. Saito, “Expressive whole-body 3d gaussian avatar,” *arXiv preprint arXiv:2407.21686*, 2024.
- [7] W. Wang, H. Yang, J. Kittler, and X. Zhu, “Single image, any face: Generalisable 3d face generation,” *arXiv preprint arXiv:2409.16990*, 2024.
- [8] Z. Qian, S. Wang, M. Mihajlovic, A. Geiger, and S. Tang, “3dgs-avatar: Animatable avatars via deformable 3d gaussian splatting,” in *Proceedings of the IEEE/CVF conference on computer vision and pattern recognition*, 2024, pp. 5020–5030.
- [9] R. Hu, X. Wang, Y. Yan, and C. Zhao, “Tgavatar: Reconstructing 3d gaussian avatars with transformer-based tri-plane,” *IEEE Transactions on Circuits and Systems for Video Technology*, 2025.

- [10] Y. Du, Y. Zhang, H.-X. Yu, J. B. Tenenbaum, and J. Wu, "Neural radiance flow for 4d view synthesis and video processing," in *Proceedings of the IEEE/CVF International Conference on Computer Vision*, 2021.
- [11] Y.-L. Liu, C. Gao, A. Meuleman, H.-Y. Tseng, A. Saraf, C. Kim, Y.-Y. Chuang, J. Kopf, and J.-B. Huang, "Robust dynamic radiance fields," in *Proceedings of the IEEE/CVF Conference on Computer Vision and Pattern Recognition*, 2023, pp. 13–23.
- [12] G. Wu, T. Yi, J. Fang, L. Xie, X. Zhang, W. Wei, W. Liu, Q. Tian, and X. Wang, "4d gaussian splatting for real-time dynamic scene rendering," in *Proceedings of the IEEE/CVF conference on computer vision and pattern recognition*, June 2024, pp. 20 310–20 320.
- [13] W. Jiang, K. M. Yi, G. Samei, O. Tuzel, and A. Ranjan, "Neuman: Neural human radiance field from a single video," in *European Conference on Computer Vision*. Springer, 2022, pp. 402–418.
- [14] C. Guo, T. Jiang, X. Chen, J. Song, and O. Hilliges, "Vid2avatar: 3d avatar reconstruction from videos in the wild via self-supervised scene decomposition," in *Proceedings of the IEEE/CVF Conference on Computer Vision and Pattern Recognition*, 2023, pp. 12 858–12 868.
- [15] W. Li, X. Pan, J. Lin, P. Lu, D. Feng, and W. Shi, "Frpgs: Fast, robust, and photorealistic monocular dynamic scene reconstruction with deformable 3d gaussians," *IEEE Transactions on Circuits and Systems for Video Technology*, 2025.
- [16] Z. Guo, W. Zhou, L. Li, M. Wang, and H. Li, "Motion-aware 3d gaussian splatting for efficient dynamic scene reconstruction," *IEEE Transactions on Circuits and Systems for Video Technology*, 2024.
- [17] M. Loper, N. Mahmood, J. Romero, G. Pons-Moll, and M. J. Black, "SMPL: A skinned multi-person linear model," *ACM Trans. Graphics (Proc. SIGGRAPH Asia)*, vol. 34, no. 6, pp. 248:1–248:16, Oct. 2015.
- [18] T. Li, T. Bolkart, M. J. Black, H. Li, and J. Romero, "Learning a model of facial shape and expression from 4D scans," *ACM Transactions on Graphics, (Proc. SIGGRAPH Asia)*, vol. 36, no. 6, pp. 194:1–194:17, 2017. [Online]. Available: <https://doi.org/10.1145/3130800.3130813>
- [19] T. Li, M. Slavcheva, M. Zollhoefer, S. Green, C. Lassner, C. Kim, T. Schmidt, S. Lovegrove, M. Goesele, R. Newcombe *et al.*, "Neural 3d video synthesis from multi-view video," in *Proceedings of the IEEE/CVF conference on computer vision and pattern recognition*, 2022, pp. 5521–5531.
- [20] Z. Li, S. Niklaus, N. Snavely, and O. Wang, "Neural scene flow fields for space-time view synthesis of dynamic scenes," in *Proceedings of the IEEE/CVF Conference on Computer Vision and Pattern Recognition*, 2021, pp. 6498–6508.
- [21] K. Park, U. Sinha, P. Hedman, J. T. Barron, S. Bouaziz, D. B. Goldman, R. Martin-Brualla, and S. M. Seitz, "Hypernerf: A higher-dimensional representation for topologically varying neural radiance fields," *ACM Trans. Graph.*, vol. 40, no. 6, dec 2021.
- [22] S. Fridovich-Keil, G. Meanti, F. R. Warburg, B. Recht, and A. Kanazawa, "K-planes: Explicit radiance fields in space, time, and appearance," in *Proceedings of the IEEE/CVF Conference on Computer Vision and Pattern Recognition*, 2023, pp. 12 479–12 488.
- [23] A. Cao and J. Johnson, "Hexplane: A fast representation for dynamic scenes," in *Proceedings of the IEEE/CVF Conference on Computer Vision and Pattern Recognition*, 2023, pp. 130–141.
- [24] Z. Yang, H. Yang, Z. Pan, and L. Zhang, "Real-time photo-realistic dynamic scene representation and rendering with 4d gaussian splatting," *arXiv preprint arXiv:2310.10642*, 2023.
- [25] J. Luiten, G. Kopanas, B. Leibe, and D. Ramanan, "Dynamic 3d gaussians: Tracking by persistent dynamic view synthesis," *arXiv preprint arXiv:2308.09713*, 2023.
- [26] J. Bae, S. Kim, Y. Yun, H. Lee, G. Bang, and Y. Uh, "Per-gaussian embedding-based deformation for deformable 3d gaussian splatting," *arXiv preprint arXiv:2404.03613*, 2024.
- [27] Z. Li, Z. Chen, Z. Li, and Y. Xu, "Spacetime gaussian feature splatting for real-time dynamic view synthesis," in *Proceedings of the IEEE/CVF Conference on Computer Vision and Pattern Recognition*, 2024, pp. 8508–8520.
- [28] T. Li, T. Bolkart, M. J. Black, H. Li, and J. Romero, "Learning a model of facial shape and expression from 4d scans." *ACM Trans. Graph.*, vol. 36, no. 6, pp. 194–1, 2017.
- [29] V. Blanz and T. Vetter, "A morphable model for the synthesis of 3d faces," in *Seminal Graphics Papers: Pushing the Boundaries, Volume 2*, 2023, pp. 157–164.
- [30] J. Romero, D. Tzionas, and M. J. Black, "Embodied hands: Modeling and capturing hands and bodies together," *arXiv preprint arXiv:2201.02610*, 2022.
- [31] T. Alldieck, M. Magnor, W. Xu, C. Theobalt, and G. Pons-Moll, "Detailed human avatars from monocular video," in *2018 International Conference on 3D Vision (3DV)*. IEEE, 2018, pp. 98–109.
- [32] B. Mildenhall, P. P. Srinivasan, M. Tancik, J. T. Barron, R. Ramamoorthi, and R. Ng, "Nerf: Representing scenes as neural radiance fields for view synthesis," *Communications of the ACM*, vol. 65, no. 1, pp. 99–106, 2021.
- [33] B. Kerbl, G. Kopanas, T. Leimkühler, and G. Drettakis, "3d gaussian splatting for real-time radiance field rendering," *ACM Transactions on Graphics*, vol. 42, no. 4, July 2023. [Online]. Available: <https://repo-sam.inria.fr/fungraph/3d-gaussian-splatting/>
- [34] T. Jiang, X. Chen, J. Song, and O. Hilliges, "Instantavatar: Learning avatars from monocular video in 60 seconds," in *Proceedings of the IEEE/CVF Conference on Computer Vision and Pattern Recognition*, 2023, pp. 16 922–16 932.
- [35] J. Zhang, X. Li, H. Zhong, Q. Zhang, Y. Cao, Y. Shan, and J. Liao, "Humanref-gs: Image-to-3d human generation with reference-guided diffusion and 3d gaussian splatting," *IEEE Transactions on Circuits and Systems for Video Technology*, 2025.
- [36] X. Chen, T. Jiang, J. Song, M. Rietmann, A. Geiger, M. J. Black, and O. Hilliges, "Fast-snarf: A fast deformer for

- articulated neural fields,” *IEEE Transactions on Pattern Analysis and Machine Intelligence*, vol. 45, no. 10, pp. 11 796–11 809, 2023.
- [37] X. Chen, Y. Zheng, M. J. Black, O. Hilliges, and A. Geiger, “Snarf: Differentiable forward skinning for animating non-rigid neural implicit shapes,” in *Proceedings of the IEEE/CVF International Conference on Computer Vision*, 2021, pp. 11 594–11 604.
- [38] G. Gafni, J. Thies, M. Zollhofer, and M. Nießner, “Dynamic neural radiance fields for monocular 4d facial avatar reconstruction,” in *Proceedings of the IEEE/CVF Conference on Computer Vision and Pattern Recognition*, 2021, pp. 8649–8658.
- [39] Z. Yu, W. Cheng, X. Liu, W. Wu, and K.-Y. Lin, “Mono-human: Animatable human neural field from monocular video,” in *Proceedings of the IEEE/CVF Conference on Computer Vision and Pattern Recognition*, 2023, pp. 16 943–16 953.
- [40] S. Peng, J. Dong, Q. Wang, S. Zhang, Q. Shuai, X. Zhou, and H. Bao, “Animatable neural radiance fields for modeling dynamic human bodies,” in *Proceedings of the IEEE/CVF International Conference on Computer Vision*, 2021, pp. 14 314–14 323.
- [41] P. Paudel, A. Khanal, A. Chhatkuli, D. P. Paudel, and J. Tandukar, “ihuman: Instant animatable digital humans from monocular videos,” *arXiv preprint arXiv:2407.11174*, 2024.
- [42] Z. Shao, Z. Wang, Z. Li, D. Wang, X. Lin, Y. Zhang, M. Fan, and Z. Wang, “Splattingavatar: Realistic real-time human avatars with mesh-embedded gaussian splatting,” in *Proceedings of the IEEE/CVF conference on computer vision and pattern recognition*, 2024, pp. 1606–1616.
- [43] J. Wen, X. Zhao, Z. Ren, A. G. Schwing, and S. Wang, “Gomavatar: Efficient animatable human modeling from monocular video using gaussians-on-mesh,” in *Proceedings of the IEEE/CVF conference on computer vision and pattern recognition*, 2024, pp. 2059–2069.
- [44] J. L. Schonberger and J.-M. Frahm, “Structure-from-motion revisited,” in *Proceedings of the IEEE conference on computer vision and pattern recognition*, 2016, pp. 4104–4113.
- [45] J. L. Schönberger, E. Zheng, J.-M. Frahm, and M. Pollefeys, “Pixelwise view selection for unstructured multi-view stereo,” in *Computer Vision—ECCV 2016: 14th European Conference, Amsterdam, The Netherlands, October 11–14, 2016, Proceedings, Part III 14*. Springer, 2016, pp. 501–518.
- [46] J. Lei, Y. Wang, G. Pavlakos, L. Liu, and K. Daniilidis, “Gart: Gaussian articulated template models,” in *Proceedings of the IEEE/CVF conference on computer vision and pattern recognition*, 2024, pp. 19 876–19 887.
- [47] S. Goel, G. Pavlakos, J. Rajasegaran, A. Kanazawa, and J. Malik, “Humans in 4d: Reconstructing and tracking humans with transformers,” in *Proceedings of the IEEE/CVF International Conference on Computer Vision*, 2023, pp. 14 783–14 794.
- [48] C. R. Qi, H. Su, K. Mo, and L. J. Guibas, “Pointnet: Deep learning on point sets for 3d classification and segmentation,” in *Proceedings of the IEEE conference on computer vision and pattern recognition*, 2017, pp. 652–660.
- [49] C. R. Qi, L. Yi, H. Su, and L. J. Guibas, “Pointnet++: Deep hierarchical feature learning on point sets in a metric space,” *arXiv preprint arXiv:1706.02413*, 2017.
- [50] Z. Wang, A. C. Bovik, H. R. Sheikh, and E. P. Simoncelli, “Image quality assessment: from error visibility to structural similarity,” *IEEE transactions on image processing*, vol. 13, no. 4, pp. 600–612, 2004.
- [51] R. Zhang, P. Isola, A. A. Efros, E. Shechtman, and O. Wang, “The unreasonable effectiveness of deep features as a perceptual metric,” in *Proceedings of the IEEE conference on computer vision and pattern recognition*, 2018, pp. 586–595.
- [52] Z. Zhu, Z. Fan, Y. Jiang, and Z. Wang, “Fsgs: Real-time few-shot view synthesis using gaussian splatting,” in *European Conference on Computer Vision*. Springer, 2025, pp. 145–163.
- [53] P. K. Diederik, “Adam: A method for stochastic optimization,” (*No Title*), 2014.
- [54] R. A. Güler, N. Neverova, and I. Kokkinos, “Densepose: Dense human pose estimation in the wild,” in *Proceedings of the IEEE conference on computer vision and pattern recognition*, 2018, pp. 7297–7306.